Biophysical Chemistry 246 (2019) 40–49

Contents lists available at ScienceDirect

Biophysical Chemistry

journal homepage: www.elsevier.com/locate/biophyschem

Photophysical and thermodynamic evaluation on the *in vitro* and *in silico* binding profile of Camptothecin with DNA

Riju K. Thomas, Surya Sukumaran, C. Sudarsanakumar*

School of Pure and Applied Physics, Mahatma Gandhi University, Kottayam, Kerala 686560, India.

HIGHLIGHTS

- The groove binding mechanisms of anti-cancer drug, CMT with ct-DNA were elucidated by various biophysical methods.
- Structural alterations reflected in the DNA double helical structure due to CMT complexation was examined using CD and FTIR analysis.
- The *in silico* molecular docking explored the orientation along with the site specificity of CMT towards DNA minor grooves.

GRAPHICAL ABSTRACT

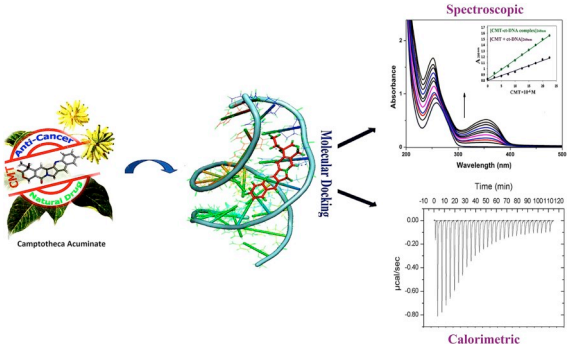

ARTICLE INFO

Keywords:
Camptothecin
ITC
Groove binding
Molecular docking

ABSTRACT

Camptothecin (CMT) is an anti-tumour alkaloid drug exhibiting selective topoisomerase-I inhibitory activity by eventually hindering dynamic functions of DNA duplex *via* initiating apoptosis. Unravelling the binding mechanism of CMT with bio macromolecular systems can offer fundamental information regarding the mechanism of actions which can lead to the design of rational proactive drugs. This study endeavoured the binding interactions of CMT with calf thymus DNA (ct-DNA) along with the structural alterations attained by the DNA duplex owing to CMT interactions through multi-spectroscopic, calorimetric and molecular docking studies. The UV–visible absorbance and fluorescence quenching studies revealed the binding strength of CMT with ct-DNA, evident from the binding constants $K_1 = 3.79 \times 10^3\,M^{-1}$ and $Kq = 2 \times 10^3\,M^{-1}$. The time-resolved lifetime measurements inferred that the quenching was static due to the non-fluorescent ground state complex formation. The dye displacement study, temperature melting and viscosity measurements established a typical non-intercalative binding mode of CMT with ct-DNA. The binding isotherm deduced from ITC was found to be spontaneous and exothermic exerting a promising ΔG value of $-6.2\,kcal\,mol^{-1}$. The thermal kinetic parameters implied that the forces primarily involved in the CMT-ct-DNA complexation are hydrogen bonding and van der Waals interactions. Moreover, the structural alterations of DNA duplex reflected in the CD and FTIR spectra could undeniably confirm the groove binding manner of CMT. The *in silico* extra precision docking study explored more accurate molecular illustrations of sequence specific minor groove binding mechanism evolved between CMT and DNA corroborating well with the experimental results. These innovative findings may shorten the path towards the development of novel and more effective CMT drug derivatives.

* Corresponding author.
E-mail address: c.sudarsan.mgu@gmail.com (C. Sudarsanakumar).

https://doi.org/10.1016/j.bpc.2018.12.004
Received 24 July 2018; Received in revised form 27 October 2018; Accepted 21 December 2018
Available online 24 December 2018

1. Introduction

Deoxyribonucleic acid (DNA), the central part of the genomic system has a significant role in the synthesis of proteins, transcription of genetic information and cell proliferation in living beings [1,2]. The renowned three-dimensional structure of DNA has been helpful to the scientific community to investigate the therapeutic effects of a wide range of drugs binding to DNA and thereby interfering with numerous dynamic functions of DNA [3]. Nowadays the molecular interactions behind the binding strategy of natural drugs with DNA have become an active area of research, providing guidance for the designing of novel drugs [4,5]. The DNA-Drug binding typically stabilizes through different modes of non-covalent interactions like electrostatic, intercalative and groove binding modes [6–8]. The electrostatic binding occurs due to the communications of the positively charged ends of ligand moieties and the negatively charged DNA backbone [9,10]. The intercalative mode of binding occurs due to π-stacking interactions of aromatic heterocyclic groups and thereby distorting the conformation of DNA backbone [10]. However, the groove binding is governed by hydrogen bonding or van der Waals interactions with nucleic acid bases devoid of further distortion in the DNA backbone [10–12]. Any alterations affecting the DNA structure leading to its dysfunction and are always linked with risk of complex diseases [13]. Cancer is one such life-threatening ailment predominantly associated with the malfunction of genetic materials and obviously leads to uncontrollable cell division and metastasis [13]. Therefore, it is necessary to reveal the exact binding mode of DNA targeted drugs to control numerous diseases by improvising systematic strategies in drug designing [12]. Elucidating the exact mode of binding action, *in vitro* designing and *in silico* screening of new potent DNA targeted drugs will be possible merely after understanding the drug-DNA interactions [4,5]. The binding mechanism of DNA as a drug target is extensively carried out by calf thymus DNA (ct-DNA) due to its availability and the predictability of its accessible chemical functional groups. The ct-DNA is a double-stranded B form of DNA having both A-T and C-G nucleotides, which is easily characterized by UV absorbance per mass. The ct-DNA is considered as highly polymerized and polydispersed, fibrous structure with negligible amount of RNA and protein content. The larger molecular weight (Mw = 8418KDa) and polydispersity index (5.2) of ct-DNA had already been reported [14]. However, the number of known DNA-based drug targets is still very limited in comparison to the protein-based drug targets hence, perceiving the binding mode of natural drugs with DNA helps to minimize its adverse side effects and can be effectually used to designate further potential drug targets [8,10].

CMT (Fig. 1) is a naturally occurring plant alkaloid found abundantly in the seeds of Chinese tree, *Camptotheca acuminate* [15,16]. It has a planar pentacyclic ring structure, that includes a pyrrolo [3, 4-β]-quinoline conjugated pyridone moiety [17,18]. CMT is a major antitumour drug that shows remarkable efficacy towards a wide range of gastric, ovarian and colorectal tumours. The chemotherapeutic role of CMT is solely governed by targeting the Topoisomerase I (Top1), which is overproduced in malignancies [19]. The selective Top1 inhibitory nature of CMT is due to the inhibition of nitric oxide biosynthesis and hence contributes to its anti-tumour activity [19,20]. The CMT will reversibly interact with Top1 cleavage complex (Top1cc) *via* a substantial encounter between the Top1cc and replication fork leading to toxicity by transient double-strand break formation [19]. The stable CMT-Top1cc ternary complex prevents DNA re-ligation and thereby initiating an apoptotic signalling pathway, eventually resulting in cell death [21]. The solubility limitations and the active lactone ring instability at physiological pH of the chemotherapeutic drug, CMT is critical because it affects the bioavailability and targeted delivery. To overcome this difficulty, multiple analogues of CMT have been developed with improved aqueous solubility and lactone stability [22,23]. Such semi-synthetic derivatives of CMT like irinotecan and topotecan are effectively used for ovarian and colorectal cancer treatments, as well as being appraised in various other clinical trials [24–26]. The interaction studies of CMT with human serum albumin had previously determined by fluorescence anisotropy spectroscopy [17,25]. The multiple binding modes of CMT towards DNA oligomers by implying a combination of calculated free energies, NOEs and chemical shifts derived from NMR spectroscopy had already been studied [27]. The pharmacological potential of CMT is limited owing to its partial solubility and in this perspective, the normal physiological absorption is also restricted irrespective of dosage quantity [15,21].

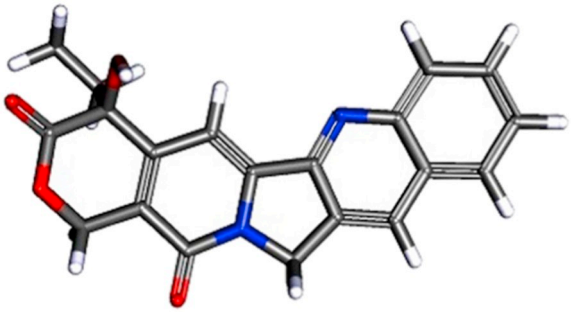

Fig. 1. Structure of camptothecin.

A clear understanding about the binding mechanism of CMT with DNA is essential to enhance its anti-cancer potential. Even though there exist contrasting findings on the interaction profile of synthetic derivatives of CMT, here we have conducted a comprehensive examination on the binding strategy of CMT with DNA by using biophysical methods such as UV–visible absorption, fluorescence spectroscopy, viscosity and melting analysis. In order to understand the intercalative mode of CMT binding with ct-DNA more clearly, the competitive dye displacement study was performed using EtBr as fuorescent probe. To attain deeper insights into the structural alterations of the B-form DNA in the presence of CMT, circular dichroism (CD) and Fourier transform infrared spectroscopy (FTIR) measurements were also performed. The thermogram evaluating the binding strength, thermodynamic parameters and binding stoichiometry behind the interaction of CMT with ct-DNA was explored by Isothermal titration calorimetry (ITC). The molecular docking analysis gave a clear evidence of the minor groove binding and sequence specificity of CMT with DNA. The *in vitro* and *in silico* binding studies of anticancer drug CMT with ct-DNA remains profound to disclose how the molecule may well be further modified to improve its biological efficacies in drug targeting and delivery.

2. Materials and methods

2.1. Materials

ct-DNA sodium Salt Type 1, Camptothecin ≥90%, Ethidium Bromide (EtBr), sodium chloride (NaCl), Tris-HCl buffer (pH 7.4) purchased from Sigma-Aldrich Chemicals. All the other solvents/chemicals were of reagent grade and used without any further purification.

2.2. Sample preparation

The stock solution of ct-DNA was prepared in Tris-HCl buffer (pH 7.4) and incubated at 4 °C for 24 h. The purity of ct-DNA solution was confirmed by the ratio of absorbance at 260 and 280 nm and was found to be higher than 1.8, indicating that ct-DNA samples were devoid of proteins [12]. The molar concentration of ct-DNA in the buffer solution was determined by the Beer-Lamberts law with the molar extinction coefficient of free DNA as 6600 M^{-1} cm^{-1} [5]. The stock solution of CMT was prepared by dissolving in 100 μL of DMSO followed by dilution with Tris-HCl buffer of pH 7.4. All reaction mixtures were prepared in 1 M-Tris-HCl buffer (pH 7.4) unless otherwise mentioned.

2.3. UV–Vis absorption spectroscopy

Absorption spectra were recorded using Agilent Technologies UV–Vis-NIR spectrophotometer (USA), provided with a temperature controller in 10 mm path length quartz cuvettes. The UV–Visible spectra of CMT and CMT-ct-DNA complexes were recorded in the wavelength range of 200-800 nm. Multiple sets of measurements were performed by maintaining constant ct-DNA (100×10^{-6} M) concentration while varying the drug concentrations (0 to 25×10^{-6} M) respectively. The reverse titration was also carried out by varying the ct-DNA concentrations (0 to 45 μM) at a constant CMT (100 μM) concentration.

2.4. Fluorescence quenching studies

Fluorescence quenching studies were performed using HORIBA Fluromax spectrofluorometer with a cuvette of 10 mm path length. The fluorescent titrations were recorded at a spectral range of 390 to 650 nm with an excitation wavelength of 370 nm by upholding a slit width of 3 nm. The titrations were done by adding increasing concentrations of ct-DNA (0-100 μM) to the system containing constant CMT concentration (100 μM). Fluorescence lifetime analyses were also performed using a Pico-second diode (Spectra-Nano-LED source S-343) with an excitation wavelength of 370 nm.

2.5. EtBr displacement studies and the role of ionic strength in CMT-ct-DNA complex

The dye displacement titrations were performed by Horiba-Fluromax spectro-fluorometer using an active probe, EtBr commonly used for the visualization of nucleic acids. The EtBr displacement assay explained the possibility of an intercalative mode of binding when excited at 530 nm with an emission spectra ranging from 545 to 750 nm respectively. The considerable alterations exhibited in the fluorescence intensities of ct-DNA-EtBr systems (ct-DNA 50 μM and EtBr 5 μM) both in the presence and absence of increasing concentrations of CMT (0-100 μM) were monitored. The influence of ionic strength within the CMT-ct-DNA complex was significantly demonstrated by varying the concentration of sodium chloride [NaCl] between 0 and 50 μM in the CMT-ct-DNA complex systems. The excitation executed at 370 nm was accomplished with emission spectra monitored between 390 and 650 nm respectively.

2.6. Isothermal titration calorimetry

The ITC was characterized at a temperature of 298.15 K using VP-ITC from Microcal (Northampton, MA, USA). Approximately 0.01 mM ct-DNA was prepared in Tris-HCl buffer. The ligand CMT of 0.2 mM concentration was dissolved in minimal volume of DMSO, further diluted into the desired concentration by adding the Tris-HCl buffer. An equal volume of DMSO was also added to the ct-DNA solution in Tris-HCl to nullify the effect of DMSO. Both the samples were degassed prior loaded into the ITC machine. A total of 30 injections were carried out at a time interval of 240 s with a stirring speed of 306 rpm. The data were fitted by the nonlinear least-square method using the ORIGIN software of Microcal. The data evolved from the thermogram was used to estimate the thermodynamic parameters such as molar enthalpy change (ΔH) and entropy change (ΔS) with the number of binding sites (n) and the affinity constant (K_b). The Gibbs free energy change (ΔG) and the entropic contribution (TΔS) was estimated from the standard equation shown below.

$$\Delta G = -RT \ln K_b = \Delta H - T\Delta S \quad (1)$$

2.7. DNA melting and viscosity measurements

The DNA melting temperature experiments were recorded on a Shimadzu UV-2500 double beam spectrometer, equipped with a temperature controller. The absorbance of the ct-DNA (30 μM) was monitored in the absence and presence of CMT (20 μM and 40 μM) at λ = 260 nm, by varying the temperature from 30 °C to 100 °C with a scan rate of 1 °C/min. The binding of CMT into the ct-DNA was further explored by viscosity measurements using Ubbelohde viscometer equipped with a digital clock (± 0.25 s). Viscosity measurements were conducted *via* maintaining the concentration of ct-DNA constant (50 μM) by varying the concentration of CMT ranging from 0 to 50 μM. The results plotted as $(\eta/\eta_o)^{1/3}$ *versus* the ratio of CMT/ct-DNA concentrations, where η is the viscosity of ct-DNA in the presence of CMT and η_o is the viscosity of ct-DNA alone.

2.8. Circular dichroism (CD)

The CD spectra were recorded using JASCO J-715 spectropolarimeter at 25 °C and the spectral measurements were carried out in the far-UV range (205-300 nm) with a scan rate of 500 nm/minute by keeping the slit width as 3 nm. In CD spectral studies, CMT solutions of different concentrations (0-100 μM) were titrated against constant ct-DNA concentration (50 μM) consecutively. The Tris-HCl buffer (pH 7.4) spectrum was subtracted from the spectra of ct-DNA and CMT-ct-DNA complexes.

2.9. FTIR analysis

The FTIR measurements of ct-DNA in the presence of CMT were carried out over a range of 1800-700 cm^{-1} using Shimadzu-1-model-IR-Prestige21, with ZnSe-ATR-crystal spectrometer from pike technologies at the room temperature. The deduction of the reference spectrum from ct-DNA and CMT-ct-DNA complex spectrum was carried out with the instrumental parameters. The background Tris-HCl buffer spectrum was recorded and digitally subtracted from all the spectra. Averages of three scans were carried out for all the samples. The molar ratios of CMT to ct-DNA were varied from 1: 20 to 1: 40 respectively.

2.10. Molecular docking studies

The *in vitro* experiments provide a clear-cut evidence regarding the binding of CMT with ct-DNA. Hence the docking studies were performed using Schrödinger maestro 9.1 software to elucidate the exact mode of CMT binding with B-DNA. The atomic coordinates of the DNAs 1BNA [d(CGCGAATTCGCG)$_2$], 2DND [d(CGCAAATTTGCG)$_2$] and 1CGC [d(CCGGCGCCGG)$_2$] obtained from Protein Data Bank (PDB) for *in silico* analysis. Here 1CGC is C-G rich, 1 BNA is a palindromic A-T and G-C dodecamer sequence and 2DND is an A-T rich dodecamer with 6 tandem A-T base pairs in the middle. The DNA duplex was prepared by protein preparation wizard module of Schrödinger programme. The water molecules from the DNA were removed and minimized by applying OPLS-3 force field. The structure of ligand, CMT was taken from PubChem (3D-CID-24360) and prepared using Lip-Prep module to generate different conformers of CMT. A grid of 15 Å was created around the DNA duplex and an extra precision (XP) method was applied for the docking analysis. In XP docking, the receptor molecule (DNA) was kept rigid whereas some degree of flexibility offered only to the ligand (CMT) to achieve its possible conformations. The maximum possible number of conformers for CMT was generated with various ionization states, tautomerism, stereochemistry and ring conformations to predict the energetically most suitable mode of binding with the DNA duplex. Based on the binding energy best-docked poses were exported and analysed.

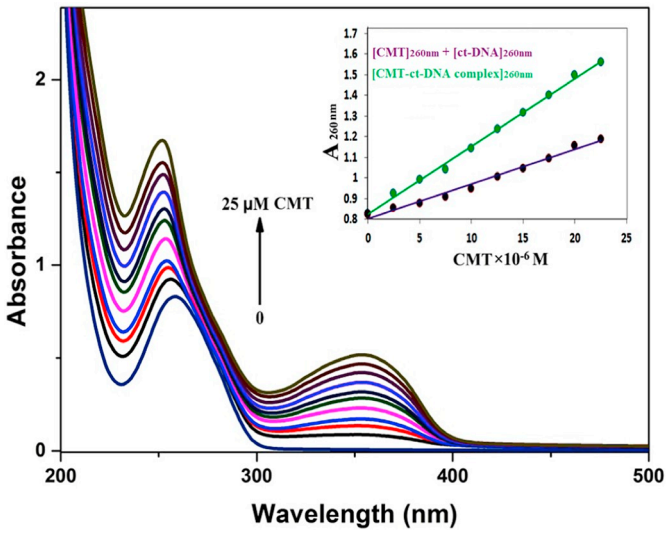

Fig. 2. UV–visible absorption spectra of ct-DNA (100 µM) in the absence and presence of different concentration of CMT (0-25 µM) (pH 7.4 1 M-Tris-HCl buffer), Inset Fig: Comparative absorbance values between CMT-ct-DNA complexes [green dots] at 260 nm and the sum of the individual absorbance value of ct-DNA and CMT [violet dots] at the wavelength 260 nm. (For interpretation of the references to colour in this figure legend, the reader is referred to the web version of this article.)

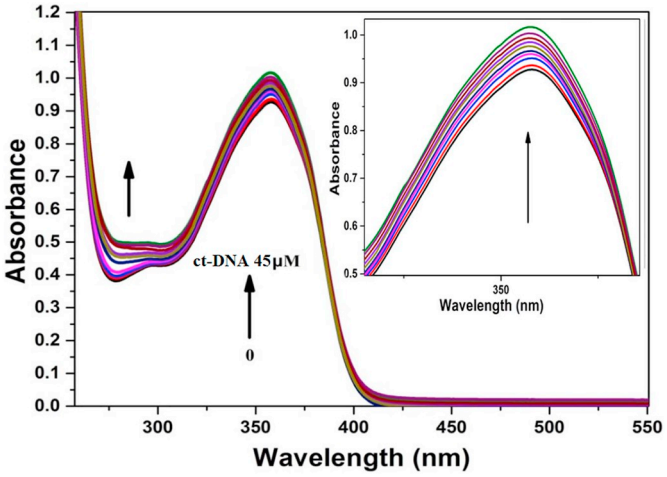

Fig. 4. UV–Vis absorption spectra of the constant concentration of CMT (100 µM) with the increasing concentration of ct-DNA (0-45 µM), Inset: enlarged image of Fig. 4 at 357 nm.

3. Results and discussions

3.1. Absorbance studies and evaluation of binding affinities

The UV–Visible absorption is a proficient method to investigate the structural alterations of bio-macromolecules due to its complex formations with drug moieties. The interaction of a ligand with DNA expresses a shift in the peak position associated with a characteristic change in the absorption maxima signifying the strength of interactions [10,28]. The hyperchromism indicates the spectral features of structural variations in the DNA double helix which originates due to typical non-intercalative nature of drugs [29,30]. When the CMT (0-25 µM) of varying concentrations were titrated into ct-DNA (100 µM) the absorbance was frequently increased with significant blue shift (λ = 260 to 256 nm) suggested a strong CMT-ct-DNA complex formation (Fig. 2). Meanwhile, the intense absorbance of CMT-ct-DNA complex at 260 nm was greater than the sum of the individual absorbance value of ct-DNA and CMT (Fig. S1) at 260 nm (inset Fig. 2), also expressed a hyperchromism after the interaction of CMT with ct-DNA. This phenomenon pointed out the non-intercalative binding mode of CMT with ct-DNA.

The binding affinity of CMT with ct-DNA was calculated by the intrinsic binding constant (K_1), using the Benesi-Hildebrand plot obtained from the following equation [31].

$$\frac{1}{\Delta A} = \frac{1}{\Delta Amax} + \frac{1}{K_1(\Delta Amax)[CMT]} \quad (2)$$

ΔA is the difference in absorbance (Ac-Ao) and [CMT] was the CMT concentration in micromolar. K_1 is obtained from intercept to the slope ratio of the linear plot. Where, A_0 and A_c are the absorbance of ct-DNA and the CMT-ct-DNA complex, respectively. The linear relationship between 1/Ac-Ao and reciprocal concentration of CMT (1/[CMT]) was used to calculate the apparent binding constant from the graph (Fig. 3a). The value of K_1 and R^2 were found to be $3.79 \times 10^3\ M^{-1}$ and 0.9975. The previous reports inferred that K_1 of intercalators were greater than in the order of $10^4\ M^{-1}$ [32,33]. Hence, it can be concluded that the binding mode of CMT with ct-DNA might be a non-intercalation binding mode and was in good agreement with the minor groove binders, luteolin and piperine [4,34].

The binding was also evaluated by the reverse titration method, where the concentration of CMT (100 µM) was kept constant by varying the concentrations of ct-DNA (0-45 µM). The double reciprocal plot of 1/(Ac-Ao) *versus* reciprocal concentration of ct-DNA (1/[ct-DNA]) was

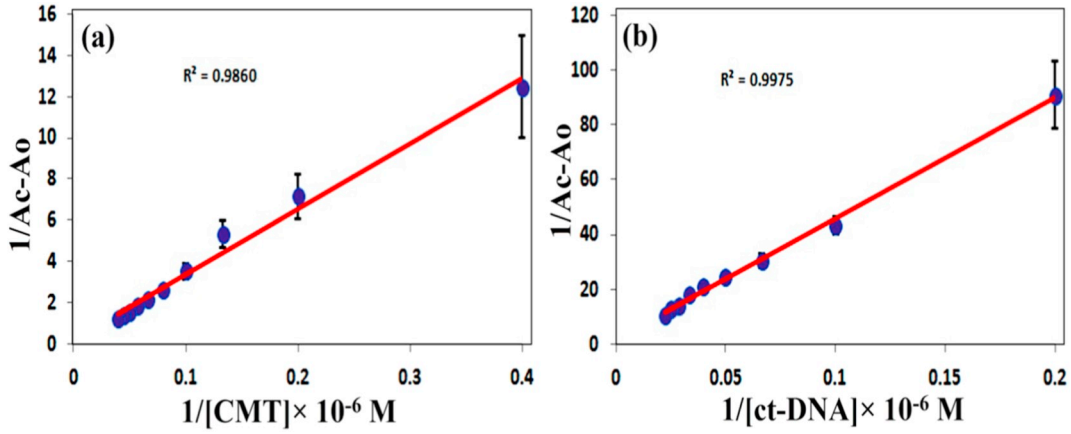

Fig. 3. (a) the plots represent 1/Ac-Ao *versus* $1/C_{CMT}$ at constant ct-DNA concentration (100 µM) with the varying concentration of CMT (0-25 µM) and (b) The plots indicate 1/Ac-Ao *versus* $1/_{Cct\text{-}DNA}$ at the constant concentration of CMT (100 µM) and with the increasing concentration of ct-DNA (0-45 µM).

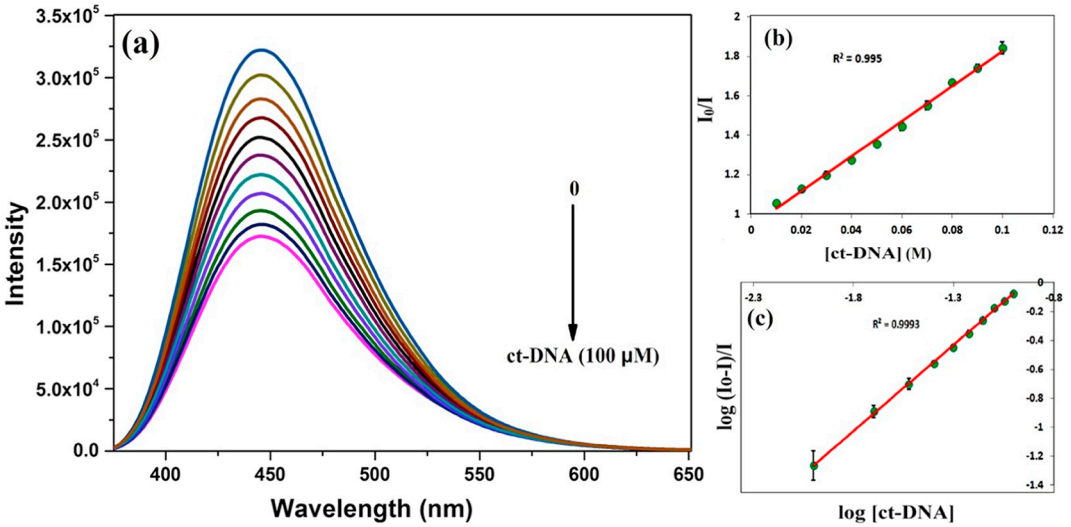

Fig. 5. (a) Emission spectra of CMT (100 μM) in the presence of increasing concentration of ct-DNA (0-100 μM) at an emission maximum of 449 nm when excited at 370 nm. (b) Stern Volmer plot of CMT with increasing concentration of ct-DNA (c) log [(I-Io)/I] *versus* log [ct-DNA] plot of the fluorescence quenching of CMT with varying concentrations of ct-DNA.

used to evaluate the binding constant (Fig. 3b). Where [ct-DNA] is the concentration of ct-DNA in micromolar concentration. The CMT exhibits an intense absorption peak at 357 nm due to the Π-Π* absorption of quinolone moiety [35]. Upon the gradual addition of ct-DNA, the absorption spectra of CMT expressed a hyperchromic effect devoid of any peak shift (Fig. 4). The hyperchromism is a spectral feature indicating the non-covalent complex formation of small molecules/drugs with ct-DNA *via* typical groove binding mode [10,36]. There was no significant shift in the absorption maxima of CMT indicating that the structural variation gained by the ligand upon its complexation with ct-DNA is minimal directing into the possibility of groove binding.

The value of K_1 obtained from eq. (2) was $3.95 \times 10^3\,M^{-1}$ with the regression coefficient 0.998. The binding constants obtained from both the absorption studies are consistent with each other and in accordance with the order of binding constants reported in other minor groove binders like sulindac and indomethacin [10,12].

3.2. Fluorescence spectroscopy

Steady-state fluorescence method was employed to study the interaction between CMT and ct-DNA [37,38]. Due to the poor endogenous fluorescence properties of ct-DNA, fluorescence emission spectra of CMT was examined for the subsequent studies. The fluorescence quenching occurs due to various inter-molecular interactions, such as energy transfer, molecular-rearrangements, ground-state complex formation and excited-state reaction [12,36]. The Fig. 5a depicted the fluorescence emission spectra of CMT with the emission maxima at 445 nm when excited at 370 nm. There was a gradual quenching of the fluorescence intensity of CMT without any shift in the emission maxima after the successive addition of ct-DNA, designates direct indication towards the CMT-ct-DNA complex formation. The quantitative analysis regarding the fluorescence alterations and quenching efficiency has been estimated in terms of Stern-Volmer quenching constant (Ksvq) which was calculated using the Stern-Volmer equation [38,39].

$$Io/I = 1 + K_{svq}[ct - DNA] \tag{3}$$

where Io is the fluorescence of CMT and I denotes the fluorescence of CMT in the presence of ct-DNA. K_{svq} is the Stern-Volmer quenching constant and [ct-DNA] is the concentration of ct-DNA in micromolar (μM). By plotting I_0/I against [ct-DNA], K_{svq} was calculated from the slope as $8 \times 10^3\,M^{-1}$ (Fig. 5b), which is consistent with the K_{svq} values of minor groove binders [10,12]. Therefore, CMT has probably a non-covalent pattern of interactions with ct-DNA, through a groove binding mode.

The Stern-Volmer constant (K_{svq}) and quenching rate constant (Kp) are related by the equation [37,39],

$$Kp = K_{svq}/\tau \tag{4}$$

where 'τ' is the average lifetime of biomolecules without quencher, the default value is nearly 10^{-8} [12,36]. The obtained quenching rate constant ($8 \times 10^{11}\,M^{-1}\,s^{-1}$) was found to be greater than the maximum scatter collision quenching constant of biomolecules ($2 \times 10^{10}\,M^{-1}\,s^{-1}$) indicated a static manner of quenching rather than dynamic [36].

For static quenching, the relationship between the fluorescence intensity and the concentration of a quencher can be described by the following equation [5,37]:

$$\log\left[\frac{Io - I}{I}\right] = logKq + nlog[ct - DNA] \tag{5}$$

where, Kq and n are the binding constant and the number of binding sites respectively. From the slope and the intercept of the plot log (Io-I)/I *versus* log [ct-DNA], the 'Kq' and 'n' were calculated as $2 \times 10^3\,M^{-1}$ and 1.2, respectively (Fig. 5c). The value of Kq in the order of $10^3\,M^{-1}$

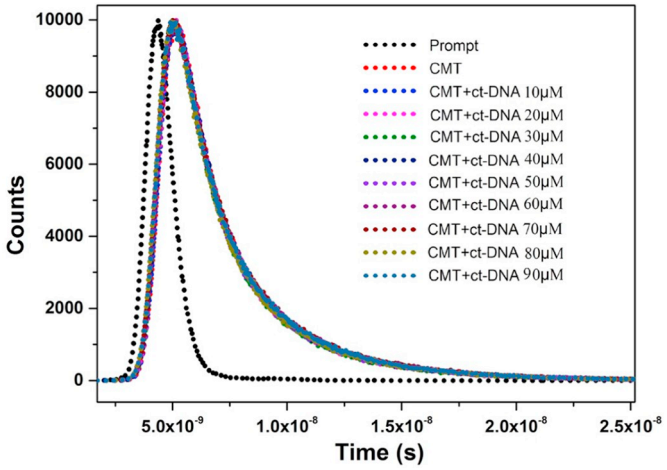

Fig. 6. Fluorescence decay of CMT in the absence and presence of ct-DNA (0-90 μM).

Table 1
Fluorescence lifetime parameters of CMT in the absence and presence of ct-DNA (0-90 μM).

DNA (μM)	$\tau_{A\ (nm)}$	$\tau_{B\ (nm)}$	$\tau_{C(nm)}$	G_1	G_2	G_3	$\tau_{m\ (\times 10s)^{-7}}$	$\chi 2$
0	1.63	0.22	4.28	41.5	14.3	44.2	2.59	0.94
10	1.65	0.27	4.27	41.3	14.1	44.6	2.63	0.95
20	1.62	0.21	4.3	42	14.2	43.8	2.60	0.94
30	1.64	0.23	4.4	42.2	14.6	43.2	2.62	0.92
40	1.67	0.25	4.2	41.3	13.8	44.9	2.60	0.91
50	1.64	0.26	4.28	41.9	13.9	44.2	2.61	0.98
60	1.68	0.23	4.3	41.5	14.1	44.4	2.61	0.94
70	1.67	0.23	4.32	41.7	14.1	44.2	2.61	0.96
80	1.65	0.27	4.28	41.3	14.2	44.5	2.61	0.95
90	1.67	0.23	4.29	41.4	14.1	44.5	2.62	0.96

at 25 °C, is consistent with the order of binding constant obtained from the UV–visible absorbance analysis, further strengthening the minor groove binding mode of CMT. The value 'Kq' is also consistent with other reported minor groove binders curcumin, sulindac and indomethacin [5,10,12].

3.3. Time-resolved fluorescence decay

Time resolved fluorescence was carried out to find the nature of fluorescence quenching. The dynamic quenching happens from the collisions between the fluorophore and quencher while the static quenching is due to the ground state complex formation between the quencher (ct-DNA) and the fluorophore (CMT) [7,38]. The fluorescence lifetime of pure CMT and CMT with different concentrations of ct-DNA (0-90 μM) were investigated (Fig. 6). Here, the decay curves of CMT and CMT-ct-DNA complex systems fitted to third order multi-exponential function using the photon counting data acquisition HORIBA software DataStation v2.4 (DAS v2.4).

The CMT involves three time constants, for the fits: $\tau_A = 1.63$ ns, $\tau_B = 0.22$ ns and $\tau_C = 4.28$ ns. The mean lifetime ($\boldsymbol{\tau_m}$) value can be calculated using the equation [37–39].

$$\boldsymbol{\tau_m} = \tau_A G_1 + \tau_B G_2 + \tau_C G_3 \quad (6)$$

where $\mathbf{G_1}$, $\mathbf{G_2}$, $\mathbf{G_3}$, $\boldsymbol{\tau_A}$, $\boldsymbol{\tau_B}$, and $\boldsymbol{\tau_C}$ are the relative amplitudes and decay times of the multi-exponential fluorescence decay. The mean lifetime of CMT obtained was 2.59×10^{-7} s and it is marginally shifted to a maximum of 2.63×10^{-7} s upon the subsequent addition of ct-DNA. There was no noticeable alteration in the lifetime values implied that the quenching was static due to the non-fluorescent ground state complex formation between CMT and ct-DNA. The decay parameters of CMT and CMT-ct-DNA were summarized in Table. 1.

3.4. The EtBr displacement studies and effects of ionic strength

EtBr is one of the prominent fluorescent probes having a phenenthridinium ring which interacts with DNA base pairs in an intercalative manner. The weak fluorescence of EtBr in aqueous solutions drastically increases due to its interaction with the DNA base pairs [12,30]. Any molecule which intercalates with DNA will compete with EtBr and substitute it from the DNA duplex, which ultimately results in fluorescence quenching of the EtBr-ct-DNA complex [10,12]. With the continuous addition of CMT to EtBr-ct-DNA systems, no significant decrease in the fluorescence intensity was monitored (Fig. 7a). This phenomenon probably occurred due to the non-replacement of EtBr from the EtBr-ct-DNA complex by the CMT, furthermore revealed a non-intercalative manner of binding.

In order to reveal the influence of electrostatic interaction, the ionic strength of CMT-ct-DNA complex system was monitored by using NaCl [10]. In the presence of increasing concentration of Na^+, the electrostatic repulsion between the negatively charged phosphate backbones on the adjacent nucleotides are reduced and thereby weakening the electrostatic interactions between ct-DNA and drugs [10,12]. The Fig. 7b presented no significant alteration in the fluorescence spectra of CMT-ct-DNA complex system in the presence of increasing concentration of NaCl, inferred that the electrostatic interaction may not played any crucial role in the complex formation. The relative variations of the

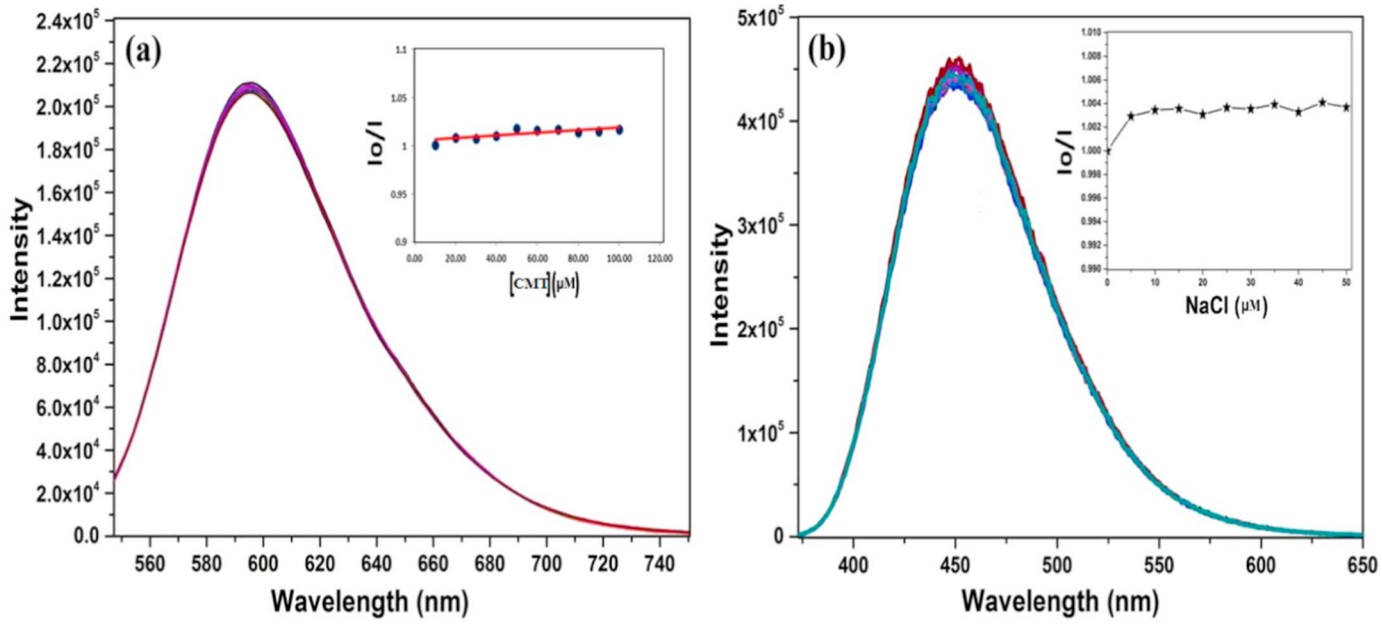

Fig. 7. (a) Competitive displacement assays: Fluorescence spectra of EtBr-ct-DNA (EtBr 5 μM) (ct-DNA 50 μM) system with CMT. The EtBr-ct-DNA complex was excited at 475 nm and its emission spectra recorded from 526 to 750 nm; Inset: Stern-Volmer plots represented the fluorescence quenching of different EtBr-ct-DNA complex by the continuous addition of CMT (0-100 μM). (b) Role of ionic strength: Fluorescence emission intensity plot of the CMT-ct-DNA complex with increasing concentration of NaCl (0-50 μM) at the excitation wavelength of 370 nm. The fluorescence emission spectra recorded in the range of 390-650 nm. Inset: Fluorescence variations in the intensity of CMT-ct-DNA system with increasing concentration of NaCl.

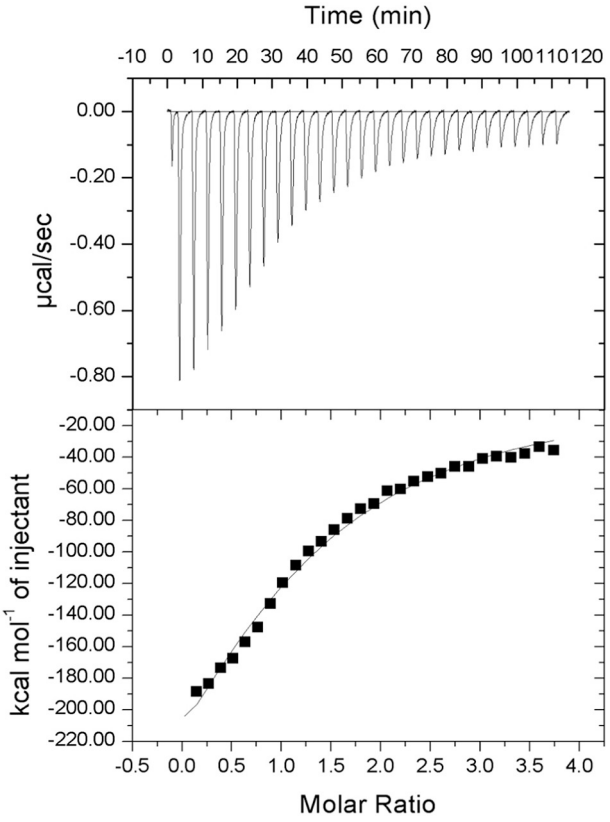

Fig. 8. The ITC profile for the interaction of CMT with the ct-DNA solution in Tris-HCl buffer, at 25 °C. Top panel signifies the heat progression due to the successive injection of CMT into the ct-DNA. The lower panel indicates the corresponding normalized heat v/s molar ratio.

Table 2
the energetic profile of the interaction of the CMT with ct-DNA obtained from the ITC at 25 °C.

Molecule	ΔH (cal/Mol)	ΔS (cal/Mol deg)	n	K_b (M^{-1})	ΔG Kcal/Mol
CMT	$-1.9 \times 10^4 \pm 0.16$	−42.9	0.95	8.5×10^4	−6.2 ± 0.45

fluorescence intensity of CMT-ct-DNA systems as a function of NaCl concentrations (inset Fig. 7b); suggested the influence of merely negligible electrostatic interactions between CMT and ct-DNA.

3.5. Isothermal titration calorimetry

ITC, a powerful sensitive technique which had been developed not only for investigating the thermodynamic parameters but also the kinetic features evolved during complex formation within biological systems [28,31]. It provides a complete thermodynamic profile of the binding such as Gibbs energy change (ΔG), entropy change during the binding reaction (TΔS), enthalpy change (ΔH) as well as binding affinity (K_b) and the number of binding sites (n) along with the intermolecular forces responsible for complex formation [10,34,37]. The corresponding heat evolution curves of CMT-ct-DNA binding were illustrated on the top panel whereas the bottom panel was sketched by rectified heat as a function of the molar ratio of CMT and ct-DNA (Fig. 8). The binding isotherm obtained when the CMT was titrated sequentially into the solution of ct-DNA was found to be exothermic in nature with binding stoichiometry $n = 0.95$, which is in accordance with the number of binding sites attained for the minor groove binders curcumin and piperine [4,5]. The value of `n` was approximately equal

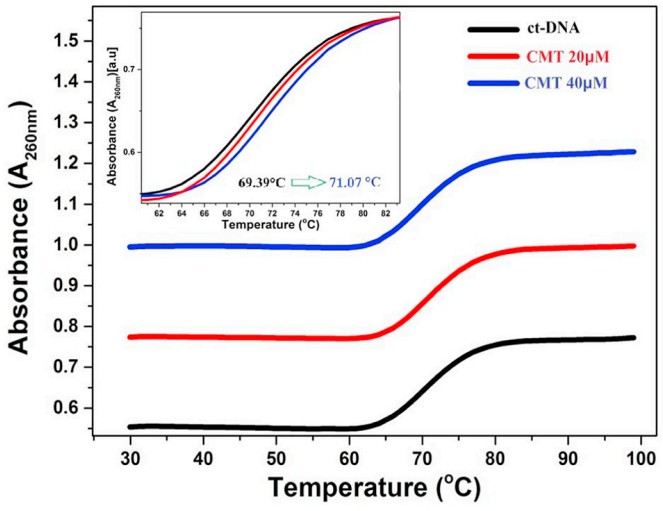

Fig. 9. Represents melting temperature (*Tm*) of ct-DNA (30 µM) in the absence and presence of CMT [20 µM–40 µM], where A_{260} is the absorbance of ct-DNA with increasing temperature (30 °C–100 °C).

to unity which inferred the existence of single binding site per nucleotide of ct-DNA [12]. The magnitudes of various thermodynamic parameters including n, K_b, ΔH, ΔS and ΔG were designated in Table 2.

The negative values of ΔS and ΔH indicate the existence of hydrogen bonds and Van der Waals interactions within the CMT-ct-DNA complex. It had already been reported that the groove binders exhibit an enthalpy-driven association with slight unfavourable entropic contributions [12,39]. The sign and magnitude of the deduced thermodynamic parameters (−ΔG,-ΔS and -ΔH) suggested that the entire process was spontaneous and enthalpy driven. The ΔG value of -6.2 kcal mol^{-1} provided an insight into the minor groove binding mode of CMT with ct-DNA. Here the thermal parameters from ITC experiment indicated a good measure of binding, which is in closer accordance with the reported values of the minor groove binders [4,5,12].

3.6. Melting temperature analysis

The DNA double helix is highly stable due to the presence of hydrogen bonding and base stacking interactions [34,40]. Melting temperature analysis is an evaluation tool to ensure denaturation effects on ct-DNA due to the breaking of hydrogen bonds between the base pairs while heating. With increasing temperature, the double helical DNA get unwound and separates into single-stranded form owing to various distortions happening to the binding forces [9–12]. The melting temperature [*Tm*] is the temperature at which half of the double helical DNA dissociates into single-stranded, which is directly correlated with the stability of the DNA duplex. The groove or electrostatic mode of binding by drug molecules does not show any significant variation in *Tm* value. On the other hand, the intercalative mode of binding raises the *Tm* value by about 5–8 °C, due to the stabilization of the DNA double helix [30,31]. The *Tm* for ct-DNA in the absence and presence of CMT was determined by monitoring the absorbance at 260 nm (A_{260nm}) as a function of temperature ranging from 30 to 100 °C (Fig. 9). The T*m* value for ct-DNA alone was recorded as 69.3 ± 0.1 °C but in the presence of CMT, the *Tm* increased to 70.13 ± 0.1 °C (20 µM) and 71.07 ± 0.1 °C (40 µM) respectively. The slight hike in the observed *Tm* might be due to the conformational alterations happened due to the groove binding of CMT with ct-DNA, which drawn out the probability of intercalative mode of binding. The negligible change in the *Tm* of CMT-ct-DNA complex, when compared to native ct-DNA disclosed a good agreement with the well-reported minor groove binders like esculetin and indomethacin [12,41].

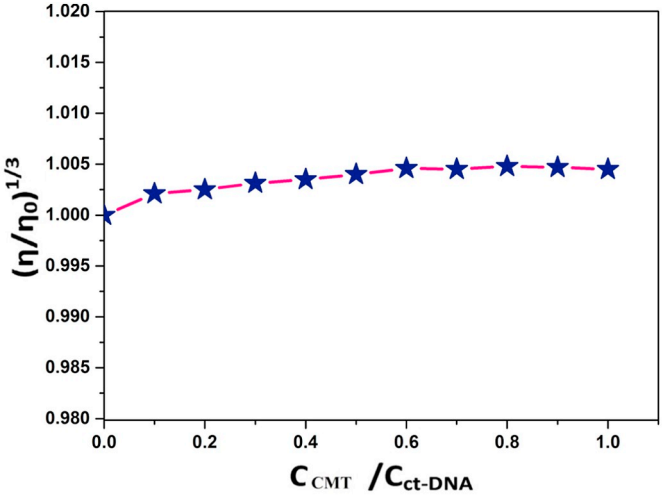

Fig. 10. Effects of increasing the concentration of CMT (0-50 μM) on the viscosity of ct-DNA solution. The concentration of ct-DNA was kept constant (50 μM) while changing the concentration of CMT.

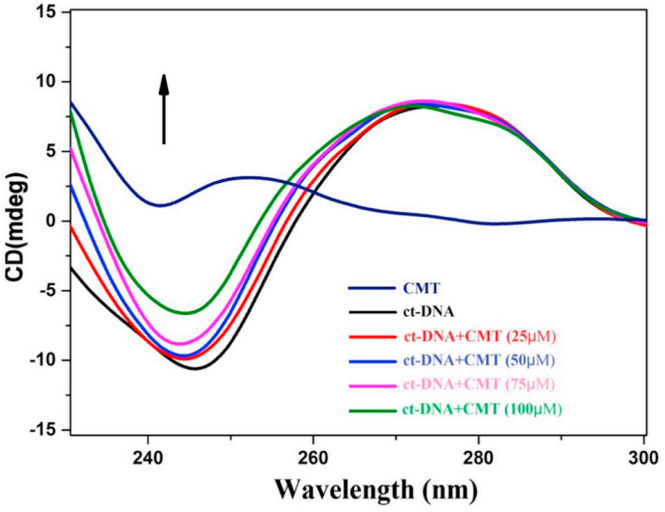

Fig. 11. Influence of varying concentrations of CMT (0-100 μM) on the CD spectra of ct-DNA (50 μM) in Tris-HCl buffer (pH 7.4) at 25 °C.

3.7. Viscosity measurements

The viscosity measurement is a most reliable technique to determine the binding modes of drugs with DNA [31]. Classical intercalators lengthen the double helical structure of DNA due to the separation of base pairs, which will, in turn, increase the viscosity of DNA solution [12,41]. However, the groove binding or electrostatic interactions cause only negligible variations in the viscosity of the DNA [10,40]. The viscosity plot of $(\eta / \eta_0)^{1/3}$ *versus* the concentration of CMT/ct-DNA was constructed to reveal alterations in the viscosity of the ct-DNA solution in the presence of CMT [Fig. 10]. In the plot, η indicates the viscosity of ct-DNA in the presence of CMT and η_0 is the viscosity of ct-DNA alone. With the subsequent additions of CMT, there was no significant alteration observed in the viscosity of the ct-DNA solution and is in better agreement with the minor groove binders, sulindac and methyldopa [10,36]. The mentioned slight variations in the DNA relative viscosity specified the bending of the ct-DNA due to its complex formation with CMT.

3.8. Circular dichroism spectroscopy

CD spectroscopy is a highly sensitive method illustrating the conformational alterations in the double helical structure of DNA while

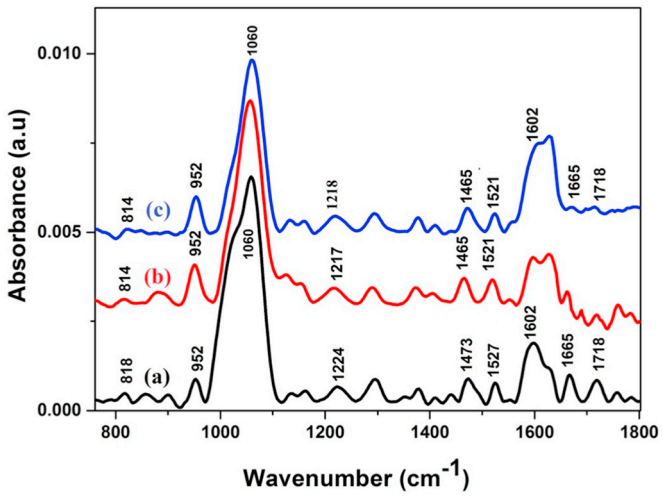

Fig. 12. FTIR spectra of (a) ct-DNA (24 mM) and CMT-ct-DNA complexes with different molar ratios of CMT to ct-DNA, (b) 1: 20 and (c) 1: 40).

forming complexes with ligands. It is being extensively used for monitoring the transformations occurring in the secondary structures of DNA, proteins and polypeptides upon their interactions with drug molecules [36,41]. The CD spectrum of ct-DNA exhibits a positive and a negative band at 276 nm and 247 nm which are attributed to the base stacking interaction and right-handed double helicity of B-DNA, respectively. These bands are extremely sensitive to explain the groove binding interaction of drugs with DNA [42–44]. In the case of groove binding, there exists very little perturbation of the helicity and base stacking bands of DNA, however in the case of intercalators, the intensities of both the bands are extensively disturbed on a wide range [10,12,41]. As evident from Fig. 11, with the progressive addition of CMT, there was no significant change in the spectral band responsible for the base stacking (276 nm) and a decrease in the intensity of band attributed to helicity of ct-DNA (247 nm). The unaltered bases stacking interactions indicated that the intercalation was not the binding strategy of CMT with ct-DNA. On the other hand, the reduced helicity of ct-DNA indicating the alteration in the ellipticity of DNA helix revealed that CMT bound to ct-DNA through the groove binding fashion like that of minor groove binder, topotecan [43].

3.9. FTIR ds-DNA spectral evaluation

FTIR spectroscopy is a prominent method established to elucidate the structural alterations of double-stranded DNA (ds-DNA) in the presence of small molecules [44]. The deviations in FTIR spectra of ds-DNA can be correlated with the specific binding sites of ligand moieties in DNA [30]. Previous reports have unravelled that ct-DNA expresses deoxyribose, phosphate and nitrogenous bases stretching vibrations. The infra-red spectrum of ct-DNA alone and CMT-ct-DNA complexes were monitored in the specific region of 750-1800 cm^{-1}. As presented in Fig. 12, the bands at 1224 cm^{-1} and 1060 cm^{-1} of ct-DNA were attributed to the phosphate asymmetric and symmetric vibrations, respectively. The frequency of the band at 952 cm^{-1} resembled the deoxy-ribose C—C and C—O stretching vibrations, and the band at 818 cm^{-1} was accredited to the phospho-diester, which is regarded as a marker band for the B-form of ct-DNA [30,44]. With the increasing concentration of CMT, both the phosphate and deoxy-ribose stretching vibrations expressed slight variations in the band position (812 cm^{-1} to 814 cm^{-1} and 1224 cm^{-1} to 1218 cm^{-1}) explored that the complex formation of CMT with ct-DNA occurred through the sugar-phosphate backbone. Furthermore, the bands at 1473 cm^{-1}, 1602 cm^{-1}, 1665 cm^{-1} and 1718 cm^{-1}were ascribed to cytosine (C), adenine (A), thymine (T) and guanine (G) stretching vibrations of ct-DNA, respectively [30,42]. The alterations in the position and intensity of these bands can be used to examine the interaction of

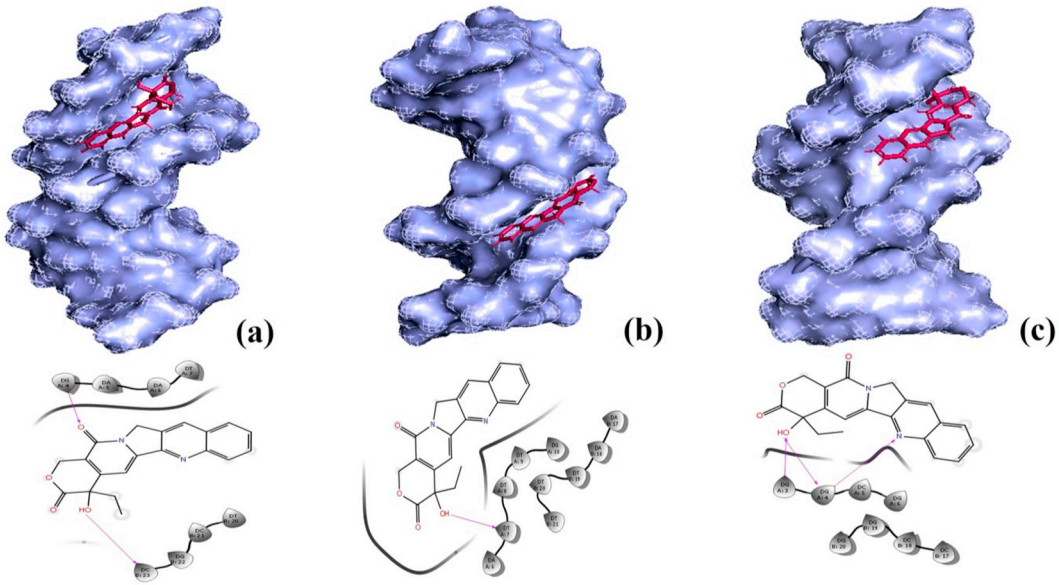

Fig. 13. Molecular docked structures representing the surface binding and two-dimensional view of hydrogen bonds (violet lines) between CMT and (a) 1BNA, (b) 2DND and (c) 1CGC. (For interpretation of the references to colour in this figure legend, the reader is referred to the web version of this article.)

CMT with four nitrogenous bases. With the increasing concentrations of CMT, the cytosine stretching vibration band was downshifted from 1473 cm^{-1} to 1465 cm^{-1}, along with a decrease in the intensities of thymine (1665 cm^{-1}) and guanine (1718 cm^{-1}) bands and an increase in the intensity of adenine (1602 cm^{-1}) band (Fig. 12). Meanwhile, the downward shift of the bands representing cytosine, deoxyribose C—C and C—O stretching vibrations are pointing to the minimal conformational alterations happened to the B-form of ct-DNA in the presence of CMT, following the trends in the CD spectral studies. Therefore, the CD and FTIR results were well supported by the UV-absorbance, fluorescence and viscosity analysis revealed that CMT is bound to ct-DNA preferentially through groove binding mode.

3.10. Molecular docking studies

Molecular docking method is a mechanistic study to predict the exact binding sites and binding affinities of small molecules with biomolecules [45,46]. The *in silico* docking retracts information correlating the structural features of receptor-ligand complexes, which can further validate the *in vitro* experimental results [10,12]. The small molecules will interact with the minor groove, while large molecules tend to recognize the major grooves of DNA [41,46]. In this study, molecular docking between CMT and 3 distinct templates of DNA duplexes were done using Schrödinger programme. The A-T rich 2DND, G-C rich 1CGC and palindromic 1BNA are B form of DNA duplexes commonly used for docking studies [5,12,14]. The CMT prepared by ligprep module was flexible to attain the different conformations, to predict the binding mode with all the three distinct templates of B-DNA duplexes and its site specificity towards A-T or G-C regions. The most favourable conformation of the docked poses were screened based on binding energy. The best-docked poses illustrating the binding of CMT in the minor grooves of B-DNA duplexes including 1BNA, 2DND and 1CGC were exported and depicted in Fig. 13. In the case of 1BNA, CMT was bound in the minor groove region between the base pairs G2•C23 and T7•A18 with a binding energy of -5.23 $kcalmol^{-1}$ (Fig. S 2(a)). The carbonyl group and one of the side chain hydroxyl groups of CMT are in hydrogen bonds with the guanine (G4) in the chain A and cytosine (C23) in the chain B of 1BNA, respectively. In 2DND, the CMT was bound in the region between A4•T21 and G10•C15 with a binding energy of -2.9 $kcalmol^{-1}$ (Fig. S 2(b)). The hydrogen bond observed in this complex is between one of the side-chain hydroxyl groups of CMT and the thymine (T7) in the A chain of 2DND. On the other hand in1CGC, CMT was bound in the minor groove between the base pairs C1•G20 and G6•C15 with a binding energy of -5.41 $kcalmol^{-1}$ (Fig. S 2(c)). One of the side-chain hydroxyl groups in CMT forms a bifurcated hydrogen bonds with G4 and G3 in chain A. Also, and nitrogen in the quinoline ring of CMT forms a hydrogen bond with G4. Among the three complexes, CMT bound in the A-T rich region of 2DND shows the lowest binding energy (-2.9 $kcalmol^{-1}$). In 1BNA the CMT bound region has both AT and GC base pairs, while in 1CGC, the bound region has only G-C base pairs. In both cases the binding energy was similar (-5.23 $kcalmol^{-1}$ and -5.41 $kcalmol^{-1}$) and is in good agreement with the binding energy from ITC measurement (-6.23 $kcalmol^{-1}$), the above values are almost double the binding energy of CMT in A-T region (2DND). Therefore, it can be stated that the CMT shows less binding preference to A-T region than the G-C and mixed regions. Hence, the *in silico* results also substantiate our experimental studies regarding the minor groove binding of CMT with ct-DNA.

4. Conclusion

This study investigated the binding pattern of CMT with ct-DNA using various biophysical approaches and unquestionably established the minor groove mode of binding. Through the UV-absorbance and steady-state fluorescence spectral analysis, the formation of CMT-ct-DNA complex was confirmed and the binding constants were obtained consistently in the order of 10^3 mol^{-1}, which was synchronized with those of the renowned minor groove binders. The EtBr-competitive dye displacement assay, temperature melting and viscosity measurements confirmed the non-intercalative binding strategy of CMT with ct-DNA. The thermal parameters obtained from the ITC favoured a negative enthalpy of binding and the reaction was spontaneous, exothermic and enthalpy driven with ΔG of-6.2$KcalM^{-1}$. The magnitudes of kinetic parameters also confirmed the presence of hydrogen bonding and Van der Waals interactions. The lifetime measurements of CMT does not express any noticeable alterations in the presence of ct-DNA, implied a static mode of quenching. The ionic strength result ruled out the possibility of electrostatic interaction between CMT and ct-DNA and was in accordance with ITC results. Moreover, the structural alterations due to CMT-ct-DNA complexation monitored by CD and FTIR spectra further strengthen the groove mode of binding between CMT and ct-DNA duplex. The *in silico* molecular docking explored the orientation along

with the site specificity of CMT towards G-C and mixed sequences of DNA minor grooves than the A-T regions. These outcomes delivered constructive information regarding the binding interactions of the bioactive CMT with ct-DNA at the molecular level, which should throw light for further designing of CMT based drugs and derivatives with higher therapeutic index.

Conflict of interest

The authors declare that there is no conflict of interest.

Acknowledgements

The authors Riju thank UGC for BSR-RFSMS and Surya acknowledge DST-SERB-National post-doctoral fellowship. We also express gratitude to Prof. M. Haridas and Prof. C. Sadasivan, Inter University Centre for Bioscience, Kannur University, Thalassery Campus, Palayad, Kerala, India for providing access to ITC and molecular docking facility.

Appendix A. Supplementary data

Supplementary data to this article can be found online at https://doi.org/10.1016/j.bpc.2018.12.004.

References

[1] S. Kashanian, Z. Shariati, H. Roshanfekr, Ghobadi DNA binding studies of 3-5-6-trichloro-2-pyridinol pesticide metabolite, DNA Cell Biol. 31 (2012) 1341–1348.
[2] R.K. Thomas, S. Sukumaran, C. Sudarsanakumar, Photobehaviour and in vitro binding strategy of natural drug, chlorogenic acid with DNA: A case of groove binding, J. Mol. Struct. 1178 (2019) 62–72.
[3] S.B. Zimmerman, The three-dimensional structure of DNA, Annu. Rev. Biochem. 51 (1982) 395–427.
[4] P. Haris, V. Mary, M. Haridas, C. Sudarsanakumar, Energetics, thermodynamics, and molecular recognition of piperine with DNA, J. Chem. Inf. Model. 55 (2015) 2644–2656.
[5] P. Haris, V. Mary, P. Aparna, K.V. Dileep, C. Sudarsanakumar, A comprehensive approach to ascertain the binding mode of curcumin with DNA, Spectrochim. Acta A Mol. Biomol. Spectrosc. 175 (2017) 155–163.
[6] G. Barone, A. Terenzi, A. Lauria, A.M. Almerico, J.M. Leal, N. Busto, B. Garcia, DNA binding of nickel (II), copper (II) and zinc (II) complexes, Structure-affinity relationships, Coord. Chem. Rev. 257 (2013) 2848–2862.
[7] R.K. Thomas, S. Sukumaran, S. Prasanth, C. Sudarsanakumar, Revealing the interaction strategy of Diosmin functionalized gold nanoparticles with ctDNA: Multi-spectroscopic, calorimetric and thermodynamic approach, J. Lumin. 205 (2019) 265–276.
[8] N. Shahabadi, L. Heidari, Binding studies of the antidiabetic drug, metformin to calf thymus DNA using multispectroscopic methods, Spectrochim. Acta A Mol. Biomol. Spectrosc. 97 (2012) 406–410.
[9] M.A. Husain, S.U. Rehman, H.M. Ishqi, T. Sarwar, M. Tabish, Spectroscopic and molecular docking evidence of aspirin and diflunisal binding to DNA: a comparative study, RSC Adv. 5 (2015) 64335–64345.
[10] M.A. Husain, H.M. Ishqi, S.U. Rehman, T. Sarwar, S. Afrin, Y. Rahman, M. Tabish, Elucidating the interaction of sulindac with calf thymus DNA: biophysical and in silico molecular modelling approach New, J. Chemother. 41 (2017) 14924–14935.
[11] S. Afrin, Y. Rahman, T. Sarwar, M.A. Husain, A. Ali, M. Tabish, Molecular spectroscopic and thermodynamic studies on the interaction of anti-platelet drug ticlopidine with calf thymus DNA, Spectrochim. Acta A Mol. Biomol. Spectrosc. 186 (2017) 66–75.
[12] M.A. Husain, H.M. Ishqi, T. Sarwar, S.U. Rehman, M. Tabish, Interaction of indomethacin with calf thymus DNA: a multi-spectroscopic, thermodynamic and molecular modelling approach, Med. Chem. Commun. 8 (2017) 1283–1296.
[13] R. Palchaudhuri, P.J. Hergenrother, DNA as a target for anticancer compounds: methods to determine the mode of binding and the mechanism of action, Curr. Opin. Biotechnol. 18 (2007) 497–503.
[14] B. Porsch, R. Laga, J. Horský, C. Koňák, K. Ulbrich, Molecular weight and polydispersity of calf-thymus DNA: static light-scattering and size-exclusion chromatography with dual detection, Biomacromolecules 10 (2009) 3148–3150.
[15] M.E. Wall, M.C. Wani, C.E. Cook, K.H. Palmer, Plant antitumor agents. I. The isolation and structure of camptothecin, a novel alkaloidal leukemia and tumor inhibitor from camptotheca acuminata, J. Am. Chem. Soc. 88 (1966) 3888–3890.
[16] M. Watanabe, K. Kawano, M. Yokoyama, Preparation of camptothecin-loaded polymeric micelles and evaluation of their incorporation and circulation stability, Int. J. Pharm. 308 (2006) 183–189.
[17] F. Fleury, A. Ianoul, M. Berjot, A. Feofanov, A.J. Alix, I. Nabiev, Camptothecin-binding site in human serum albumin and protein transformations induced by drug binding, FEBS Lett. 14 (1997) 215–220.
[18] P. Botella, E. Rivero-Buceta, Safe approaches for camptothecin delivery: Structural analogues and nanomedicines, J. Control. Release 247 (2017) 28–54.
[19] R.G. Shao, C.X. Cao, W. Nieves-Neira, M.T. Dimanche-Boitrel, E. Solary, Y. Pommier, Activation of the Fas pathway independently of Fas ligand during apoptosis induced by camptothecin in p53 mutant human colon carcinoma cells, Oncogene 20 (2001) 1852.
[20] X. Shen, J. Chen, R. Qiu, X. Fan, Y. Xin, Effect of camptothecin on inducible nitric oxide synthase expression in the colon cancer SW480 cell line, Oncol. Lett. 10 (2015) 3157–3160.
[21] V. Sharma, T.A. Lansdell, S. Peddibhotla, J.J. Tepe, Sensitization of tumor cells toward chemotherapy: enhancing the efficacy of camptothecin with imidazolines, Chem. Biol. 11 (2004) 1689–1699.
[22] Z.L. Song, H.L. Chen, Y.H. Wang, M. Goto, W.J. Gao, P.L. Cheng, S.L. Morris-Natschke, Y.Q. Liu, G.X. Zhu, M.J. Wang, K.H. Lee, Design and synthesis of novel PEG-conjugated 20 (S)-camptothecin sulfonylamidine derivatives with potent in vitro antitumor activity via Cu-catalyzed three-component reaction, Bioorg. Med. Chem. Lett. 25 (2015) 2690–2693.
[23] J.W. Singer, R. Bhatt, J. Tulinsky, K.R. Buhler, E. Heasley, P. Klein, P. de Vries, Water-soluble poly-(l-glutamic acid)–Gly-camptothecin conjugates enhance camptothecin stability and efficacy in vivo, J. Control. Release 74 (2001) 243–247.
[24] V.J. Venditto, E.E. Simanek, Cancer therapies utilizing the camptothecins: a review of the in vivo literature, Mol. Pharm. 7 (2010) 307–349.
[25] S. Kruszewski, Interaction of camptothecin with human serum albumin determined by fluorescence anisotropy spectroscopy, Acta Pol. Pharm. 73 (2016) 29.
[26] S. Sirikantaramas, A. Meeprasert, T. Rungrotmongkol, H. Fuji, T. Hoshino, H. Sudo, M. Yamazaki, K. Saito, Structural insight of DNA topoisomerases I from camptothecin-producing plants revealed by molecular dynamics simulations, Phytochemistry 113 (2015) 50–56.
[27] W. Bocian, R. Kawęcki, E. Bednarek, J. Sitkowski, A. Pietrzyk, M.P. Williamson, P.E. Hansen, L. Kozerski, Multiple binding modes of the camptothecin family to DNA oligomers, Chem. Eur. J. 10 (2004) 5776–5787.
[28] R.K. Thomas, S. Prasanth, T.V. Vineeshkumar, C. Sudarsanakumar, Calorimetric and spectroscopic studies to monitor the interaction of L-cysteine functionalized selenium nanoparticles with calf thymus DNA, Adv. Sci. Lett. 24 (2018) 5624–5628.
[29] M. Sirajuddin, S. Ali, A. Badshah, Drug–DNA interactions and their study by UV–Visible, fluorescence spectroscopies and cyclic voltammetry, J. Photochem. Photobiol. 124 (2013) 1–19.
[30] S. Huang, F. Zhu, Q. Xiao, Y. Liang, Q. Zhou, W. Su, Thermodynamic investigation of the interaction between the [(η 6-p-cymene) Ru (benzaldehyde-N 4-phenylthiosemicarbazone) Cl] Cl anticancer drug and ctDNA multispectroscopic and electrochemical studies, RSC Adv. 5 (2015) 42889–42902.
[31] S. Pramanik, S. Chatterjee, A. Saha, P.S. Devi, G.S. Kumar, Unraveling the interaction of silver nanoparticles with mammalian and bacterial DNA, J. Phys. Chem. B 120 (2016) 5313–5324.
[32] Y. Cao, X.W. He, Studies of interaction between safranine T and double helix DNA by spectral methods, Spectrochim. Acta A Mol. Biomol. Spectrosc. 54 (1998) 883–892.
[33] G. Zhang, P. Fu, L. Wang, M. Hu, Molecular spectroscopic studies of farrerol interaction with calf thymus DNA, J. Agric. Food Chem. 59 (2011) 8944–8952.
[34] V. Mary, P. Haris, M.K. Varghese, P. Aparna, C. Sudarsanakumar, Experimental probing and molecular dynamics simulation of the molecular recognition of DNA duplexes by the flavonoid luteolin, J. Chem. Inf. Model. 57 (2017) 2237–2249.
[35] M.R. di Nunzio, B. Cohen, A. Douhal, Structural photodynamics of camptothecin, an anticancer drug in aqueous solutions, J. Phys. Chem. A 115 (2011) 5094–5104.
[36] N. Shahabadi, M. Maghsudi, Multi-spectroscopic and molecular modeling studies on the interaction of antihypertensive drug; methyldopa with calf thymus DNA, Mol. BioSyst. 10 (2014) 338–347.
[37] S. Prasanth, C. Sudarsanakumar, Elucidating the interaction of L-cysteine-capped selenium nanoparticles and human serum albumin: spectroscopic and thermodynamic analysis, New J. Chem. 41 (2017) 9521–9530.
[38] S. Prasanth, D.R. Raj, T.V. Vineeshkumar, R.K. Thomas, C. Sudarsanakumar, Exploring the interaction of L-cysteine capped CuS nanoparticles with bovine serum albumin (BSA): a spectroscopic study, RSC Adv. 6 (2016) 58288–58295.
[39] S. Prasanth, D.R. Raj, R.K. Thomas, T.V. Vineeshkumar, C. Sudarsanakumar, A systematic investigation on the interaction of l-cysteine functionalised Mn3O4 nanoparticles with lysozyme, RSC Adv. 6 (2016) 105010–105020.
[40] S. Das, S. Chatterjee, S. Pramanik, P.S. Devi, G. Kumar, A new insight into the interaction of ZnO with calf thymus DNA through surface defects, J. Photochem. Photobiol. B 178 (2018) 339–347.
[41] T. Sarwar, M.A. Husain, S.U. Rehman, H.M. Ishqi, M. Tabish, Multi-spectroscopic and molecular modelling studies on the interaction of esculetin with calf thymus DNA, Mol. BioSyst. 11 (2015) 522–531.
[42] S. Agarwal, D.K. Jangir, R. Mehrotra, Spectroscopic studies of the effects of anticancer drug mitoxantrone interaction with calf-thymus DNA, J. Photochem. Photobiol. 120 (2013) 177–182.
[43] H. Joshi, A. Sengupta, K. Gavvala, P. Hazra, Unraveling the mode of binding of the anticancer drug topotecan with dsDNA, RSC Adv. 4 (2014) 1015–1024.
[44] S. Agarwal, D.K. Jangir, P. Singh, R. Mehrotra, Spectroscopic analysis of the interaction of lomustine with calf thymus DNA, J. Photochem. Photobiol. B 130 (2014) 281–286.
[45] M.V. Koonammackal, U.V.N. Nellipparambil, C. Sudarsanakumar, Molecular dynamics simulations and binding free energy analysis of DNA minor groove complexes of curcumin, J. Mol. Model. 17 (2011) 2805–2816.
[46] M.J. Tomy, C.S. Sharanya, K.V. Dileep, S. Prasanth, A. Sabu, C. Sadasivan, M. Haridas, Derivatives form better lipoxygenase inhibitors than piperine: in vitro and in silico study, Chem. Biol. Drug Des. 85 (2015) 715–721.